Validation of a combined image derived input function and venous sampling approach for the quantification of [18F]GE-179 PET binding in the brain ☆

Marian Galovic [a,b,c], Kjell Erlandsson [d], Tim D. Fryer [e], Young T. Hong [e], Roido Manavaki [f], Hasan Sari [d,g], Sarah Chetcuti [h], Benjamin A. Thomas [d], Martin Fisher [e], Selena Sephton [e], Roberto Canales [e], Joseph J Russell [e], Kerstin Sander [i], Erik Årstad [i], Franklin I. Aigbirhio [e], Ashley M. Groves [d], John S. Duncan [b,c], Kris Thielemans [d], Brian F. Hutton [d], Jonathan P. Coles [h,1], Matthias J. Koepp [b,c,1,*], for the NEST investigators

[a] Department of Neurology, Clinical Neuroscience Center, University Hospital Zurich, Zurich, Switzerland
[b] Department of Clinical and Experimental Epilepsy, UCL Queen Square Institute of Neurology, University College London, London, UK
[c] MRI Unit, Chalfont Centre for Epilepsy, UK
[d] Institute of Nuclear Medicine, University College London, London, UK
[e] Wolfson Brain Imaging Centre, Department of Clinical Neurosciences, University of Cambridge, Cambridge, UK
[f] Department of Radiology, University of Cambridge, Cambridge, UK
[g] Athinoula A. Martinos Center for Biomedical Imaging, Department of Radiology, Massachusetts General Hospital and Harvard Medical School, Charlestown, MA, USA
[h] Division of Anaesthesia, Department of Medicine, University of Cambridge, Cambridge, UK
[i] Centre for Radiopharmaceutical Chemistry, University College London, London, UK

ARTICLE INFO

ABSTRACT

Blood-based kinetic analysis of PET data relies on an accurate estimate of the arterial plasma input function (PIF). An alternative to invasive measurements from arterial sampling is an image-derived input function (IDIF). However, an IDIF provides the whole blood radioactivity concentration, rather than the required free tracer radioactivity concentration in plasma. To estimate the tracer PIF, we corrected an IDIF from the carotid artery with estimates of plasma parent fraction (PF) and plasma-to-whole blood (PWB) ratio obtained from five venous samples. We compared the combined IDIF+venous approach to gold standard data from arterial sampling in 10 healthy volunteers undergoing [18F]GE-179 brain PET imaging of the NMDA receptor. Arterial and venous PF and PWB ratio estimates determined from 7 patients with traumatic brain injury (TBI) were also compared to assess the potential effect of medication. There was high agreement between areas under the curves of the estimates of PF ($r = 0.99$, $p<0.001$), PWB ratio ($r = 0.93$, $p<0.001$), and the PIF ($r = 0.92$, $p<0.001$) as well as total distribution volume (V_T) in 11 regions across the brain ($r = 0.95$, $p<0.001$). IDIF+venous V_T had a mean bias of -1.7% and a comparable regional coefficient of variation (arterial: $21.3 \pm 2.5\%$, IDIF+venous: $21.5 \pm 2.0\%$). Simplification of the IDIF+venous method to use only one venous sample provided less accurate V_T estimates (mean bias 9.9%; $r = 0.71$, $p<0.001$). A version of the method that avoids the need for blood sampling by combining the IDIF with population-based PF and PWB ratio estimates systematically underestimated V_T (mean bias -20.9%), and produced V_T estimates with a poor correlation to those obtained using arterial data ($r = 0.45$, $p<0.001$). Arterial and venous blood data from 7 TBI patients showed high correlations for PF ($r = 0.92$, $p = 0.003$) and PWB ratio ($r = 0.93$, $p = 0.003$). In conclusion, the IDIF+venous method with five venous samples provides a viable alternative to arterial sampling for quantification of [18F]GE-179 V_T.

---

1. Introduction

We recently described the first-in-human use of $[^{18}F]GE$-179, a PET radioligand selectively binding to the open (i.e. activated) *N*-methyl-D-aspartate (NMDA) receptor complex (McGinnity et al., 2014). NMDA receptors are not only involved in memory and synaptogenesis, but also have a proposed role in excitotoxicity and might contribute to epilepsy, Alzheimer's and Huntington's disease, and psychosis (Bordji et al., 2010; Cooke and Bliss, 2006; Fan and Raymond, 2007; McGinnity et al., 2015; Olney et al., 1999; Rothman and Olney, 1995). NMDA receptor blockers have been used to treat seizures, Alzheimer's disease or refractory depression (Lipton, 2006; Murrough et al., 2013; Pellock et al., 2006). We showed increased $[^{18}F]GE$-179 uptake in brains of people with epilepsy, pointing to an increased activation of NMDA receptors (McGinnity et al., 2015). Recent in vivo blocking experiments showed specificity of $[^{18}F]GE$-179 for the phencyclidine site as a use-dependent marker of NMDA receptor activation (Vibholm et al., 2020).

Several ongoing studies are using $[^{18}F]GE$-179 PET but a wide utilisation is limited by the need for arterial blood sampling for quantification of tracer binding. Blood sampling from the radial artery is invasive and associated with discomfort, bruising and a small risk of haemorrhage or thrombosis (Zanotti-Fregonara et al., 2011a). Simplification of PET methodology is needed before such imaging is successfully translated into routine clinical practice.

Suitable non-invasive methods for the quantification of $[^{18}F]GE$-179 binding are currently not available. There is no suitable reference region devoid of NMDA receptors (McGinnity et al., 2014), and in a prior study by McGinnity et al., neither standardised uptake value (SUV) nor use of a population-based arterial input function provided accurate quantification (McGinnity et al., 2018). Regional SUV calculated over the interval of 80 to 90 min after tracer injection had a Spearman's correlation coefficient of 0.78 in comparison with total distribution volume (V_T) quantified using a measured arterial input function (AIF). A higher correlation ($\rho = 0.90$) was found between regional V_T estimated using a population-based AIF and those using the measured AIF, but there was still large variability between the two methods as demonstrated by Bland–Altman plots. Importantly, both SUV and population-based AIF methods failed to replicate findings obtained using an AIF in patients with epilepsy (McGinnity et al., 2015).

As an alternative, quantification of PET data using an image-derived input function (IDIF) has been proposed as a non-invasive approach. Practical challenges remain regarding the identification of blood vessels, correction for partial volume effects, especially in the presence of subject motion, and image noise. Furthermore, the IDIF only estimates the radioactivity concentration in whole blood. Additional correction is required by the plasma-to-whole blood (PWB) radioactivity concentration ratio, and, depending on the tracer, additional correction for tracer binding to plasma proteins and/or the parent fraction of the tracer in plasma if radio-labelled metabolites are present in blood (Zanotti-Fregonara et al., 2011a). Methods validated with one tracer or scanner set-up might not be generalizable and need to be re-validated for each specific study (Zanotti-Fregonara et al., 2011b).

We have previously proposed a procedure to estimate the IDIF with a novel partial volume correction (PVC) approach using single target correction (Erlandsson and Hutton, 2014) and we validated the method using $[^{18}F]$fluorodeoxyglucose (FDG) PET (Sari et al., 2017). However, for tracers whose PWB ratio does not indicate unity, and/or with binding to plasma proteins and/or radio-labelled metabolites in blood, this method must be used in conjunction with a method for determining the appropriate correction factors.

The combination of an IDIF with venous samples was proposed to allow for correction for plasma parent fraction and PWB ratio (Zanotti-Fregonara et al., 2011a). For brain PET this approach has only been validated for a few radiotracers. As an example, an IDIF with three venous samples was used to generate the input function for the quantification of $[^{18}F]FDG$ PET (Chen et al., 2007). Another study used the IDIF in conjunction with six venous samples to quantify serotonin-1A receptors with $[carbonyl-^{11}C]WAY$-100635 PET (Hahn et al., 2012).

Here, for $[^{18}F]GE$-179 we combine the above IDIF estimation method with discrete venous samples that allow correction for plasma parent fraction and PWB ratio. We validated the combined IDIF + venous procedure against gold standard data from arterial sampling in 10 healthy volunteers. We assessed two variants of the IDIF + venous approach, using either five venous samples acquired across the scan duration or a simplified version using a single late venous sample. In addition to these approaches, we also assessed the performance of a method that does not require venous sampling, whereby the IDIF is corrected with population-based estimates of parent fraction and PWB ratio.

To validate our findings in patients, we compared parent fraction, PWB ratio, and whole blood radioactivity concentration determined from arterial and venous samples in a cohort of subjects with traumatic brain injury (TBI).

2. Material and methods

We studied 10 healthy volunteers (mean age 40 ± 9 years; 9 male) at Addenbrooke's Hospital in Cambridge, United Kingdom. As a validation cohort for the comparison of correction factors determined from arterial and venous sampling, we also included 7 patients with TBI (mean age 40 ± 15 years; 6 male) at Addenbrooke's Hospital. Four of these subjects were scanned within the first week after TBI and were receiving anaesthetic medication to facilitate intensive care management at the time of the scan; the remaining three were scanned several months after TBI. Volunteers provided informed consent, and assent was obtained from patient representatives with consent at follow-up if capacity was regained. Studies were conducted in accordance with the Declaration of Helsinki, and the study was approved by a National Research Ethics Committee and the UK Administration of Radioactive Substances Advisory Committee.

2.1. Data acquisition

PET data were acquired on a GE Discovery 690 PET/CT scanner (GE Healthcare, Waukesha, USA) for 90 min after injection of a target 185 MBq of $[^{18}F]GE$-179 (mean $\pm$ SD: 178 ± 8 MBq). List mode data were histogrammed into 58 time frames, each of which were reconstructed using the PROMIS 3D filtered backprojection algorithm (Kinahan and Rogers, 1988) into a $192 \times 192 \times 47$ matrix with a voxel size of $2 \text{ mm} \times 2 \text{ mm} \times 3.27 \text{ mm}$. The PET data were corrected for dead time, randoms, normalization, attenuation, scatter, and radioactive decay. Attenuation correction was performed using information from a low dose CT scan.

Arterial blood from the radial artery was continuously sampled for the first 6.5 min of the scan with an Allogg ABSS on-line detector (Allogg AB, Mariefred, Sweden), with two discrete samples (30 s and 4.5 min) taken beyond the on-line counter for cross-calibration against the well counter and PWB ratio determination. Discrete arterial samples were also taken directly from the arterial cannula at 10, 15 and 20 min post-injection, and at 10 min intervals thereafter. Venous samples were collected through a cannula placed in a vein in the antecubital fossa opposite the injection site at 7, 12, 22, 42, and 62 min following injection. The radioactivity concentration in whole blood and plasma for all discrete blood samples was determined with a Hidex Triathler well counter (Hidex, Turku, Finland) cross-calibrated to the PET/CT scanner. The fraction of parent tracer in plasma for 6 arterial plasma samples (4.5, 10, 20, 40, 60, and 90 min post-injection) and all five venous samples was determined using HPLC analysis. The fraction of radioactivity in plasma bound to plasma proteins was estimated by centrifugation of arterial plasma samples (0.5, 4.5, 10, 20, 40, 60 and 90 min post-injection) with a 1:1 addition of acetonitrile, followed by measurement of the radioactivity in the supernatant. The ratio of the radioactivity in
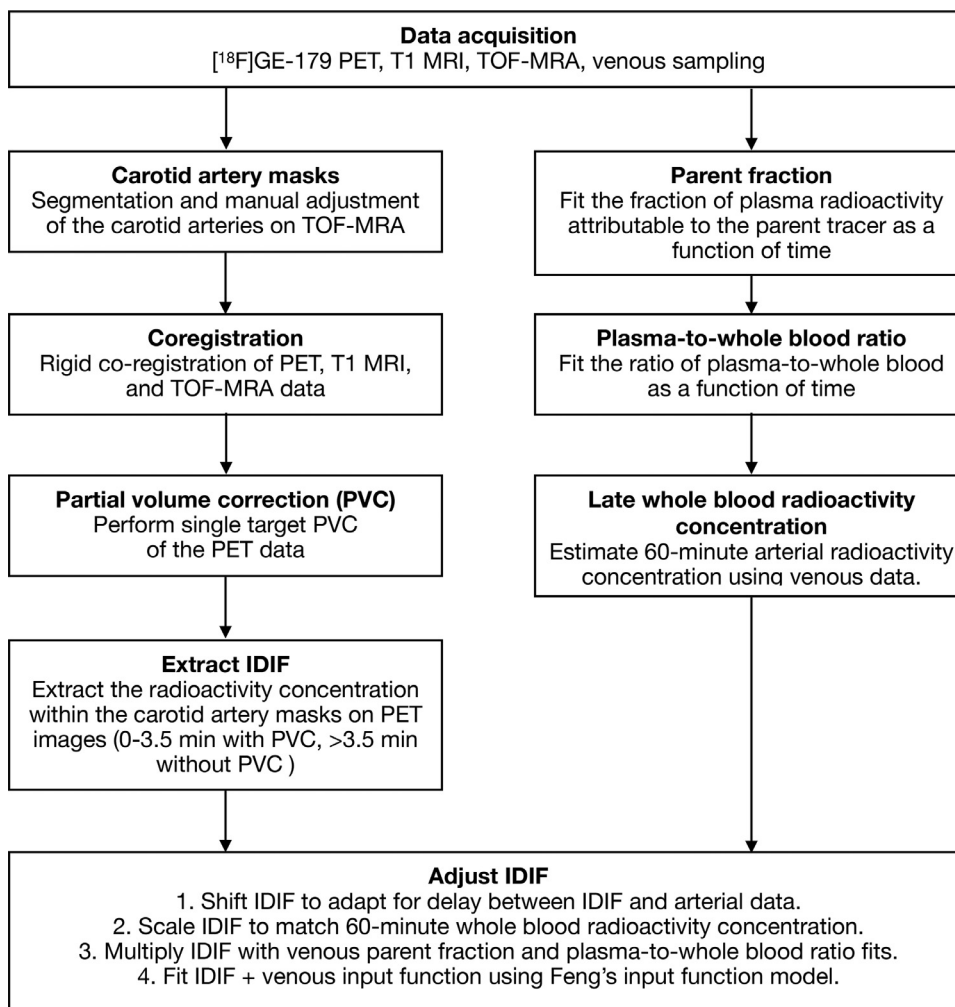
Data acquisition
[¹⁸F]GE-179 PET, T1 MRI, TOF-MRA, venous sampling

Carotid artery masks
Segmentation and manual adjustment of the carotid arteries on TOF-MRA

Parent fraction
Fit the fraction of plasma radioactivity attributable to the parent tracer as a function of time

Coregistration
Rigid co-registration of PET, T1 MRI, and TOF-MRA data

Plasma-to-whole blood ratio
Fit the ratio of plasma-to-whole blood as a function of time

Partial volume correction (PVC)
Perform single target PVC of the PET data

Late whole blood radioactivity concentration
Estimate 60-minute arterial radioactivity concentration using venous data.

Extract IDIF
Extract the radioactivity concentration within the carotid artery masks on PET images (0-3.5 min with PVC, >3.5 min without PVC)

Adjust IDIF
1. Shift IDIF to adapt for delay between IDIF and arterial data.
2. Scale IDIF to match 60-minute whole blood radioactivity concentration.
3. Multiply IDIF with venous parent fraction and plasma-to-whole blood ratio fits.
4. Fit IDIF + venous input function using Feng's input function model.

the supernatant to that in the plasma sample represented the unbound fraction.

Each healthy volunteer underwent 3T brain MRI on a Siemens Trio or Skyra system (Siemens Healthineers, Erlangen, Germany). The MR protocol included a high-resolution volumetric T1-weighted sequence (MPRAGE), as well as an arterial time-of-flight magnetic resonance angiography (TOF-MRA) sequence that included the carotid arteries.

2.2. Estimation of the IDIF

The steps involved in the production of the IDIF + venous input function are summarised in Fig. 1. For segmentation of carotid arteries in healthy volunteers, we applied a semi-automated region-growing algorithm with intensity constraints implemented in MRI-cron (https://people.cas.sc.edu/rorden/mricron/index.html) to TOF-MRA scans, that provide an excellent separation of arteries from background tissue. We manually adjusted all segmentations in a slice-by-slice manner to segment the internal carotid artery (cervical, petrous, and cavernous segments) and visible parts of the common carotid artery only. Other arteries, e.g. the vertebral arteries, were not segmented because their smaller size increases the potential for partial volume effects. We excluded the carotid syphon and cerebral segment of the internal carotid artery because of the sigmoid vessel shape and proximity to parts of the temporal lobe that might make intra-vessel signal estimates less accurate and more prone to spill-in effects from brain tissue.

We used the linear registration algorithm implemented in Statistical Parametric Mapping 12 (SPM12,

Wellcome Centre for Human Neuroimaging, London, https://www.fil.ion.ucl.ac.uk/spm/software/spm12/) to co-register dynamic PET and T1-weighted MRI to TOF-MRA images. We used the single target partial volume correction method with 10 iterations to correct for spill-out and spill-in effects due to the small size of carotid arteries compared to the scanner resolution (Sari et al., 2017). PVC is particularly important to correctly quantify arterial radioactivity concentration in the peak following tracer injection. The method is of limited value during steady state with comparable radioactivity concentrations between soft tissues and blood vessels, and it can increase noise in the images. Thus, we used PVC for the initial 3.5 min after tracer injection, i.e. from injection until the time when tissue and blood radioactivity reached a steady state based on mean input curves, to capture the radioactivity peak and obtained uncorrected values for the remainder of the acquisition to reduce the impact of noise introduced by PVC.

Next, we determined a mean delay between radioactivity arriving in the carotid arteries and detected in blood drawn from the radial artery, as described previously (Sari et al., 2017). We shifted the IDIF for each participant curve to match the activity obtained from the radial artery and determined a mean delay of 16.4 ± 4.5 s that was subsequently applied to the IDIF for all participants, as described previously (Sari et al., 2017).

Lastly, we implemented a scaling step to adjust the image-derived measurements to venous blood radioactivity. We correlated late (62 min) venous samples with the corresponding arterial radioactivity measurements, because the correlation between arterial and venous ra-

dioactivity concentration increases with time after tracer injection, and modelled the venous to arterial radioactivity concentration conversion using a linear model. We then scaled each subject's image-derived measurements to match this target value.

2.3. Blood data fitting

We used in-house software (UCL Institute of Nuclear Medicine) running in MATLAB 9.2 (The MathWorks Inc) to fit PWB ratios, parent fractions and input functions. For each participant, the PWB ratio as a function of post-injection time t was fitted with a function as follows:

$$PWB(t) = e^{-x_1 \cdot t} \cdot x_2 + x_3$$

Where $x_1 \ldots x_3$ are the model parameters (all > 0).

For each participant, the fraction of plasma radioactivity attributable to the parent tracer [^{18}F]GE-179 as a function of time t was fitted with a Hill type function (Gunn et al., 1998) as follows:

$$PF(t) = 1 + \frac{t^{x_1} \cdot (x_2 - 1)}{t^{x_1} + x_3}$$

where $x_1 \ldots x_3$ are the model parameters; $0 < x_1$, $0 \leq x_2 < 1$, $0 < x_3$. Additionally, we evaluated the effect of reducing venous sampling to only the late sample obtained 62 min after the injection. This approach required determination of population-based estimates of the x_1 and x_3 parameters that determine the shape of PWB ratio and parent fraction curves. The remaining x_2 parameter, mainly determining the amplitude of the curve, was then estimated using the single venous sample. The remaining blood data processing was left unchanged.

Lastly, we performed an analysis without venous sampling. We used population-based estimates of PWB ratio and parent fraction that were obtained using the mean arterial data in healthy volunteers. The IDIF scaling step was not performed for this method.

After correction for PWB ratio and parent fraction, the input function (arterial, IDIF + venous, IDIF + population) was fitted with Feng's input function model (Feng et al., 1993), which consists of the sum of a gamma-variate function and two exponentials.

Arterial whole blood radioactivity concentration for Figs. 3 and 8C was fitted using Feng's input function. Venous whole blood radioactivity concentration (w) for Figs. 3 and 8C was fitted with the following function:

$$w(t) = \frac{v_7 + 4v_7 e^{-v_{12}t}}{v_{22} + (1 - v_{22})e^{-v_{42}(t-v_{62})}}$$

where v_t are the measured venous whole blood radioactivity concentrations at time point t.

2.4. Regional kinetic modelling

We parcellated brain structures on T1-weighted MRI scans in healthy volunteers using an algorithm based on Geodesic Information Flows (GIF) (Cardoso et al., 2015) freely available within the NiftyWeb service tool (UCL Centre for Medical Image Computing; http://niftyweb.cs.ucl.ac.uk/). We combined regions of the GIF-atlas to produce 11 distinct brain regions representative for different cortical, subcortical, white matter, and infratentorial structures that might reflect different patterns of brain tracer binding (McGinnity et al., 2014).

Dynamic PET images were corrected for head motion using a posthoc frame-to-frame realignment method, implemented in SPM12. For each subject, an early frame with high signal-to-noise ratio and little evidence of movement was selected as the reference frame and all subsequent frames were rigidly realigned to this reference. The frames within the first 3 min after radioligand injection were not realigned due to a low signal-to-noise ratio.

Next, we linearly co-registered the realigned PET with the T1-weighted MRI using SPM12. We corrected the PET images for partial volume effects using the iterative Yang method (Erlandsson et al., 2012)

implemented in the PET-PVC toolbox (Thomas et al., 2016) guided by structural tissue information based on the modified GIF parcellation. We extracted time-activity curves of the parcellated PV-corrected regions and modelled the regional data using a 2-brain-compartment 4-rate-constant (2c4k) kinetic model with a variable blood volume component as described previously (McGinnity et al., 2014). Total volume of distribution (V_T) in mL/cm^3 was estimated for each region as a metric of tracer binding.

2.5. Statistical analysis

Data are displayed as mean $\pm$ standard deviation or mean (95% confidence interval). We calculated the area under the curve (AUC) for the fits of parent fractions, PWB ratios, and tracer plasma input functions for the whole scan length, i.e. 90 min. We compared AUCs, radioactivity concentrations, and regional V_T estimates between arterial, IDIF + venous, and IDIF + population data using Pearson's correlation coefficient (r). Bland–Altman plots were used to compare V_T estimates. We estimated the regional and global coefficient of variation (CoV) for V_T estimates modelled using arterial sampling or IDIF-based data and compared them with an independent t-test.

2.6. Data availability

Data and the MATLAB scripts used in this publication are available upon reasonable request from the authors, whereas a formal data sharing agreement will be required.

3. Results

3.1. Plasma protein binding

The percentage of arterial plasma radioactivity bound to plasma proteins had low inter-subject variability (mean 9.4% $\pm$ 1.5% for healthy volunteers, 8.2% $\pm$ 1.5% for patients), as well as low intra-scan standard deviation (2.8% $\pm$ 0.8% for healthy volunteers, 2.3% $\pm$ 1.0% for patients). These data indicate that binding to plasma proteins can be well approximated by a fixed factor of 9%, simplifying the protocol by obviating the need for direct measurement. Given the invariant nature of this factor, it was not included in the comparison of arterial and IDIF-based methods given below.

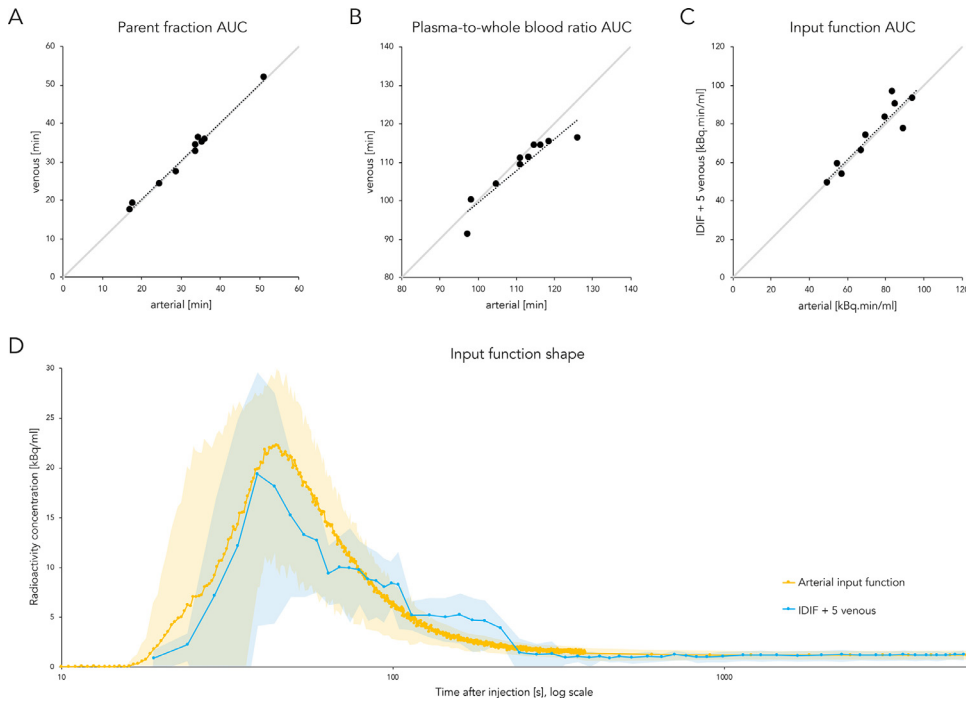### 3.2. Comparison of arterial sampling and IDIF +5 venous samples in healthy volunteers

The demographic characteristics of the 10 healthy volunteers studied are listed in Table 1. There was a high correlation between the AUC of the fits to arterial (mean 31 $\pm$ 10 min) and venous (mean 31 $\pm$ 10 min) parent fraction measurements ($r = 0.99$, $p<0.001$, Fig. 2A). There was also a high correlation between the AUC of arterial (mean 111 $\pm$ 9 min) and venous (mean 109 $\pm$ 8 min) PWB ratio measurements ($r = 0.93$, $p<0.001$, Fig. 2B).

The difference between arterial and venous whole blood radioactivity concentration decreased with time after injection (Fig. 3A). Correlations between fitted arterial and venous whole blood radioactivity concentrations at five different timepoints are shown in Fig. 3B–F. The highest correlation was observed between the fitted 60-min arterial and venous whole blood radioactivity concentrations ($r = 0.99$, $p<0.001$, Fig. 3F). The correlation between the measured 60-min arterial (1.23 $\pm$ 0.29 kBq/ml) and measured 62-min venous (1.17 $\pm$ 0.29 kBq/ml) whole blood radioactivity concentration was similarly high ($r = 0.99$, $p<0.001$). We fitted a linear model to estimate the measured 60-min arterial whole blood radioactivity concentration from the measured 62-min venous whole blood radioactivity concentration (Arterial$_{60\text{-min}}$ = Venous$_{62\text{-min}}$ * 0.987 + 0.082); this was later applied to calibrate the IDIF.

Table 1
Characteristics of healthy volunteers.

ID	Injected activity [MBq]	Age [years]	Sex	Ethnicity
CAM 01	179	36	M	European
CAM 02	173	42	M	European
CAM 03	180	43	M	European
CAM 04	177	28	M	European
CAM 05	196	39	M	European
CAM 06	181	61	M	South Asian
CAM 07	165	27	M	Australian
CAM 08	177	43	M	European
CAM 09	179	47	F	European
CAM 10	171	38	M	European
Overview	Mean 178 ± 8	Mean 40 ± 10	90% male 10% female	80% European 20% Other

M, male; F, female.

Fig. 2. Comparison of arterial and IDIF + 5 venous measurements in healthy volunteers.
Comparison of the area under the fitted curve (AUC) for arterial and venous parent fraction (**panel A**) and plasma-to-whole blood ratio (**panel B**), together with the final input function (**panel C**). On each plot the dotted line is the linear regression fit, the grey line indicates the line of unity. The mean arterial and IDIF + 5 venous input functions are displayed in **panel D,** with the light orange and blue areas denoting the corresponding 95% confidence intervals.
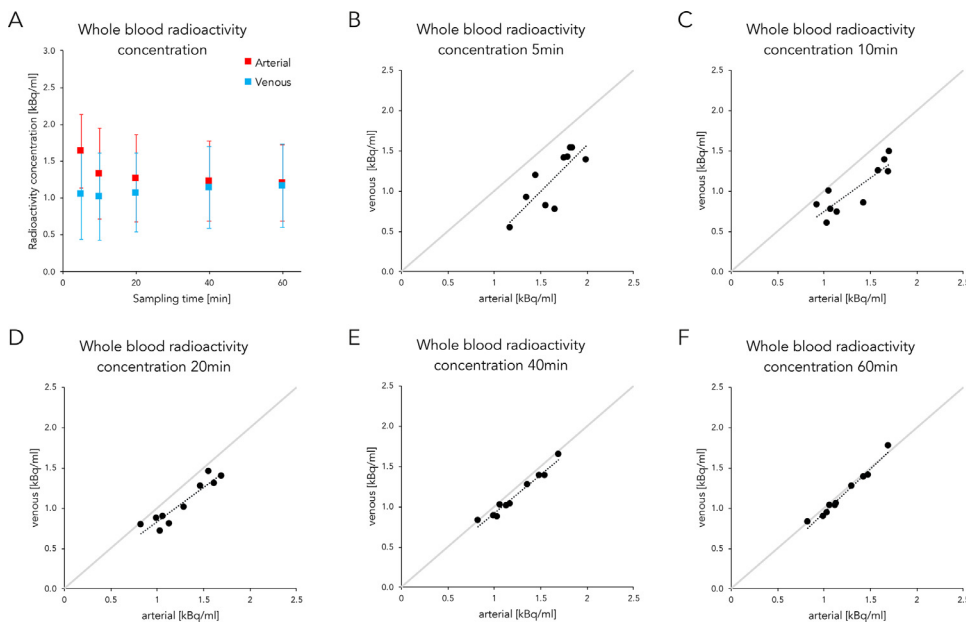
Fig. 3. Comparison of arterial and venous whole blood radioactivity concentrations in healthy volunteers.
Arterial and venous fitted whole blood radioactivity concentrations are displayed in **panel A**. The values were obtained by fitting a function to the measured data. Vertical bars denote 95% confidence intervals. Scatter plots of arterial vs. venous fitted whole blood radioactivity concentration 5, 10, 20, 40, and 60 min post-injection are displayed in **panels B to F**. On each plot the dotted line is the linear regression fit, the grey line indicates the line of unity.

Table 2
Regional V_T estimates across the healthy volunteer cohort obtained using an input function from arterial sampling or an image-derived input function in conjunction with five venous samples or a single venous sample.

	AIF		IDIF + 5 venous samples				IDIF + 1 venous sample			
	V_T estimate (mean ± SD)	CoV (%)	V_T estimate (mean ± SD)	CoV (%)	r coefficient	p value	V_T estimate (mean ± SD)	CoV (%)	r coefficient	p value
WM brain	9.2 ± 2.1	23.2	9.0 ± 2.0	21.8	0.94	<0.001	9.3 ± 1.7	18.1	0.76	0.01
WM cerebellum	9.3 ± 2.0	21.4	9.2 ± 1.9	20.9	0.94	<0.001	9.6 ± 1.7	17.8	0.68	0.03
GM cerebellum	8.8 ± 1.9	21.5	8.8 ± 1.9	22.1	0.96	<0.001	9.4 ± 1.8	19.5	0.69	0.03
Brainstem	8.7 ± 1.7	19.1	8.6 ± 1.8	20.4	0.94	<0.001	9.0 ± 1.7	18.5	0.63	0.05
Thalamus	11.9 ± 2.6	21.5	12.0 ± 2.6	21.7	0.95	<0.001	13.8 ± 2.4	17.7	0.71	0.02
Putamen	11.3 ± 2.5	22.3	11.2 ± 2.5	22.5	0.97	<0.001	12.3 ± 2.5	20.5	0.72	0.02
Precentral gyrus	9.2 ± 1.9	21.0	8.8 ± 1.8	20.8	0.89	0.001	10.8 ± 2.3	21.7	0.47	0.17
Parahippocampal gyrus	8.6 ± 2.3	27.2	8.4 ± 2.2	26.5	0.93	<0.001	9.3 ± 3.5	37.4	0.86	0.002
Occipital lobe	9.2 ± 1.7	18.2	9.0 ± 1.7	18.6	0.92	<0.001	10.7 ± 1.9	17.6	0.44	0.21
Precuneus	10.0 ± 1.9	19.3	9.7 ± 2.0	20.6	0.92	<0.001	12.0 ± 2.6	22.0	0.52	0.13
Insular cortex	10.1 ± 1.9	19.3	9.9 ± 2.0	20.4	0.94	<0.001	11.5 ± 2.4	20.9	0.52	0.12
Overall	9.7 ± 2.2	21.3 ± 2.5	9.5 ± 2.2	21.5 ± 2.0	0.95	<0.001	10.7 ± 2.7	21.1 ± 5.7	0.71	<0.001

AIF, arterial input function; IDIF, image-derived input function; V_T, volume of distribution given in mL/cm^3; CoV, coefficient of variation; r coefficient, Pearson's correlation coefficient; SD, standard deviation; WM, white matter; GM, grey matter.
The CoV of V_T estimates is given for each region per method (AIF, IDIF + 5 venous sample, or IDIF + 1 venous sample). The correlation of V_T estimates obtained with IDIF + 5 venous samples or IDIF + 1 venous sample compared with the gold standard, i.e. data modelled using an AIF, is given per region as the Pearson's correlation coefficient r and p value.
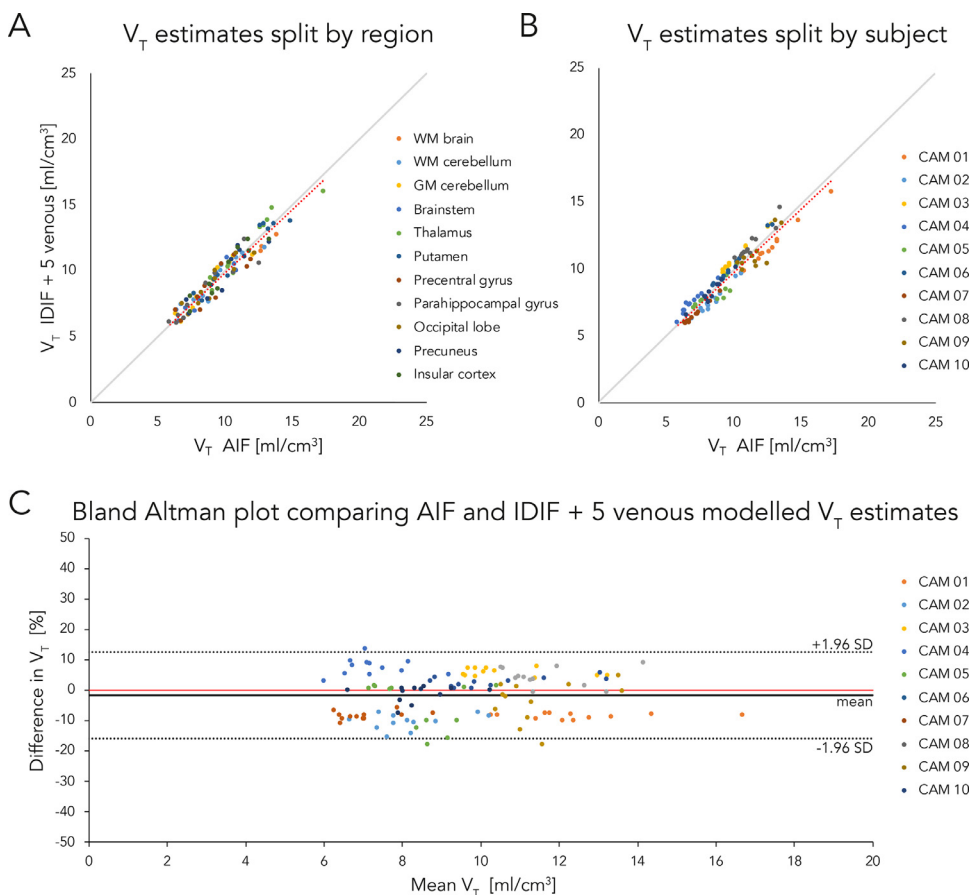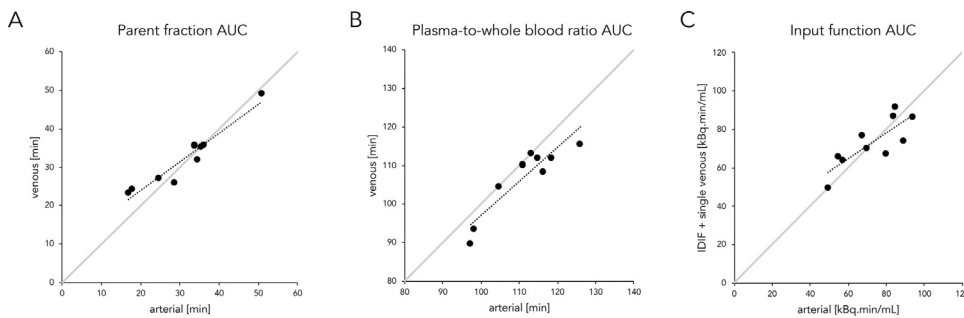

Fig. 4. Comparison of total volume of distribution estimates modelled with arterial or IDIF + 5 venous input functions in healthy volunteers.
Scatter plots of total volume of distribution (V_T) estimates obtained with arterial (AIF) and IDIF + venous input functions are displayed in **panel A** (split by region) and **B** (split by subject). The red dotted line is the linear regression fit, the grey line indicates the line of unity. **Panel C** displays a Bland–Altman plot comparing V_T estimates modelled with arterial and IDIF + venous input functions. The thick black line is the mean bias of the V_T estimates modelled using an IDIF + venous input function, the dotted black lines denote the 95% confidence intervals.

There was a high correlation of the AUC of fitted tracer plasma input functions from arterial sampling (73 ± 16 kBq min/ml) and IDIF+venous (74 ± 17 kBq min/ml, r = 0.92, p<0.001, Fig. 2C). A plot of arterial and image-derived calibrated and delay-corrected whole blood radioactivity concentrations is displayed in Fig. 2D and shows good overlap between the curves.

Regional V_T estimates obtained using arterial or IDIF + venous input functions are presented in Table 2. There was a high correlation between 110 (11 regions in 10 subjects) V_T estimates modelled with arterial or IDIF + venous data (mean V_T: arterial 9.7 ± 2.2 vs. IDIF + ve-

nous 9.5 ± 2.2, r = 0.95, p<0.001). The mean correlations remained high when splitting the data per region (mean r 0.94 ± 0.02, Fig. 4A) or per subject (mean r 0.94 ± 0.08, Fig. 4B). A Bland–Altman plot comparing V_T estimates obtained using arterial or IDIF + venous data is displayed in Fig. 4C. There was a small between-method mean difference of V_T estimates of −1.7%, with 95% limits of agreement ranging from −15.9% to 12.4%. The regional coefficients of variation of V_T for arterial and IDIF + venous modelled data were comparable (mean V_T CoV: arterial 21.3% ± 2.5% vs. IDIF + venous 21.5% ± 2.0%, t = −0.8, p = 0.46).

Fig. 5. Comparison of arterial and IDIF + single venous sample measurements in healthy volunteers.

Comparison of the area under the fitted curve (AUC) for arterial and single venous sample parent fraction (**panel A**) and plasma-to-whole blood ratio (**panel B**), together with the final input function (**panel C**). The dotted line is the linear regression fit, the grey line indicates the line of unity.
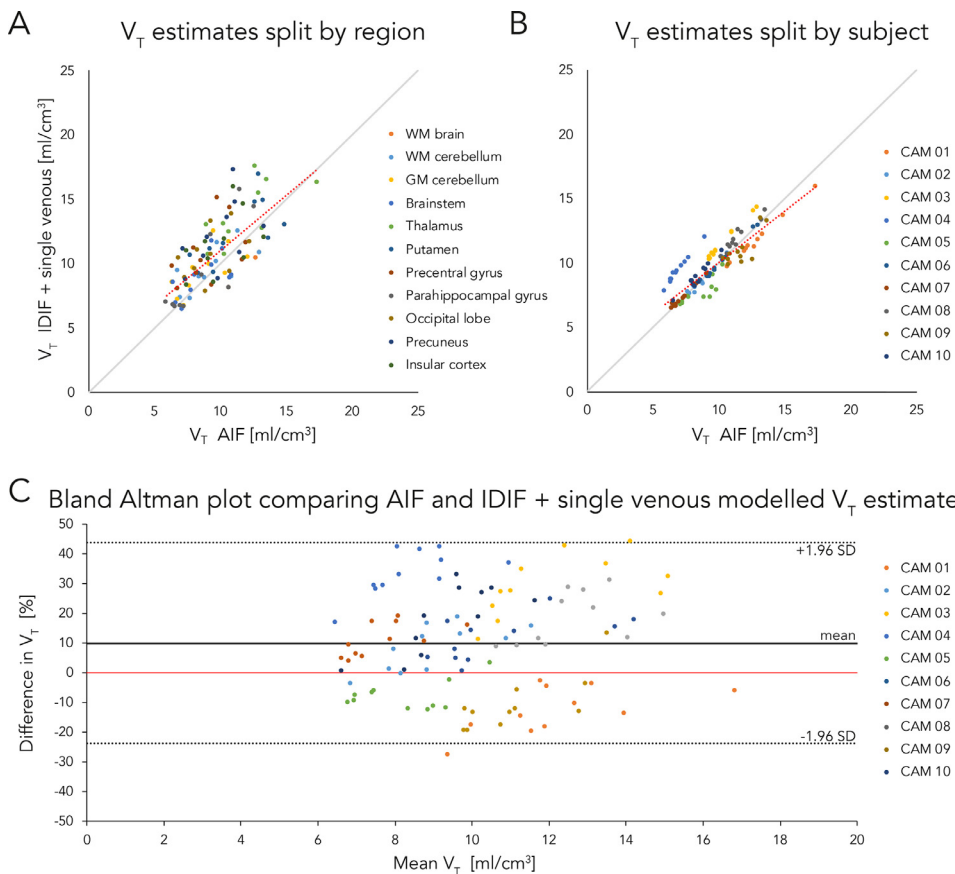
Fig. 6. Comparison of total volume of distribution estimates modelled with arterial or IDIF + single venous sample input functions in healthy volunteers.

Scatter plots of total volume of distribution (V_T) estimates obtained with arterial (AIF) and IDIF + single venous sample input functions are displayed in **panel A** (split by region) and **B** (split by subject). The red dotted line is the linear regression fit, the grey line indicates the line of unity. **Panel C** displays a Bland–Altman plot comparing V_T estimates modelled with arterial and IDIF + single venous sample input functions. The thick black line is the mean bias of the V_T estimates modelled with an IDIF + single venous sample input function, the dotted black lines denote the 95% confidence intervals.

3.3. Comparison of arterial sampling and IDIF + 1 venous sample in healthy volunteers

We also assessed the performance of a simplified IDIF + venous approach that only used a single 62-min venous sample. Compared to the IDIF + 5 venous samples method, with the simplified single venous sample version there was a lower correlation between the AUC of parent fraction measurements (single venous sample 32 ± 8 vs. arterial 31 ± 10 min, $r = 0.96$, $p<0.001$, Fig. 5A), PWB ratio estimates (single venous sample 107 ± 9 vs. arterial 111 ± 9 min, $r = 0.91$, $p<0.001$, Fig. 5B) and tracer plasma input functions (single venous sample 73 ± 13 vs. arterial 73 ± 16 kBq min/mL, $r = 0.81$, $p = 0.005$, Fig. 5C).

Regional V_T estimates obtained using the IDIF + single venous sample input function method are presented in Table 2. There was a lower correlation between arterial and IDIF + single venous sample modelled data (mean V_T: arterial 9.7 ± 2.2 vs. IDIF + single venous 10.7 ± 2.7, $r = 0.71$, $p<0.001$). The mean correlations were also lower when splitting the data per region (mean r 0.64 ± 0.13, Fig. 6A) or per subject (mean r 0.89 ± 0.08, Fig. 6B). The Bland Altman plot detected a mean

difference of V_T estimates of 9.9%, with 95% limits of agreement ranging from −23.9% to 43.7% (Fig. 6C). The simplified IDIF + single venous sample modelled data had similar coefficients of variation of V_T compared to arterial-based data (mean V_T CoV IDIF + single venous 21.1% ± 5.7%, $t = 0.2$, $p = 0.87$).

### 3.4. Comparison of arterial sampling and IDIF + population in healthy volunteers

We evaluated the performance of the IDIF + population method, which does not require venous sampling. Regional V_T estimates obtained using this method are presented in Table 3. There was a low correlation between V_T determined from arterial and IDIF + population input functions (mean V_T: arterial 9.7 ± 2.2 vs. IDIF + population 7.9 ± 2.3, $r = 0.45$, $p<0.001$). The mean correlations were also lower when splitting the data per region (mean r 0.29 ± 0.14, Fig. 7A) or per subject (mean r 0.85 ± 0.12, Fig. 7B). The Bland Altman plot showed a mean difference of V_T estimates of −20.9%, with 95% limits of agreement ranging from −69.5% to 27.7% (Fig. 7C). Data modelled using

Table 3

Regional V_T estimates across the healthy volunteer cohort obtained using an input function from arterial sampling or an image-derived input function with population-based correction factors.

	AIF		IDIF + population			
	V_T estimate (mean ± SD)	CoV (%)	V_T estimate (mean ± SD)	CoV (%)	*r* coefficient	*p* value
WM brain	9.2 ± 2.1	23.2	6.5 ± 1.5	22.5	0.25	0.49
WM cerebellum	9.3 ± 2.0	21.4	6.9 ± 1.5	21.4	0.26	0.47
GM cerebellum	8.8 ± 1.9	21.5	7.1 ± 1.7	23.6	0.34	0.32
Brainstem	8.7 ± 1.7	19.1	6.5 ± 1.6	25.0	0.32	0.37
Thalamus	11.9 ± 2.6	21.5	10.2 ± 2.4	23.6	0.31	0.38
Putamen	11.3 ± 2.5	22.3	9.2 ± 2.5	27.5	0.43	0.22
Precentral gyrus	9.2 ± 1.9	21.0	8.1 ± 1.9	23.9	0.15	0.68
Parahippocampal gyrus	8.6 ± 2.3	27.2	6.7 ± 2.4	35.5	0.60	0.07
Occipital lobe	9.2 ± 1.7	18.2	8.0 ± 1.6	20.2	0.06	0.86
Precuneus	10.0 ± 1.9	19.3	9.1 ± 2.5	27.8	0.28	0.43
Insular cortex	10.1 ± 1.9	19.3	8.5 ± 2.2	26.0	0.22	0.54
Overall	9.7 ± 2.2	21.3 ± 2.5	7.9 ± 2.3	25.2 ± 4.3	0.45	<0.001

AIF, arterial input function; IDIF, image-derived input function; V_T, volume of distribution given in mL/cm³; CoV, coefficient of variation; *r* coefficient, Pearson's correlation coefficient; SD, standard deviation; WM, white matter; GM, grey matter.
The CoV of V_T estimates is given for each region per method (AIF, IDIF + population). The correlation of V_T estimates obtained with IDIF + population compared with the gold standard, i.e. data modelled using an AIF, is given per region as the Pearson's correlation coefficient *r* and *p* value.
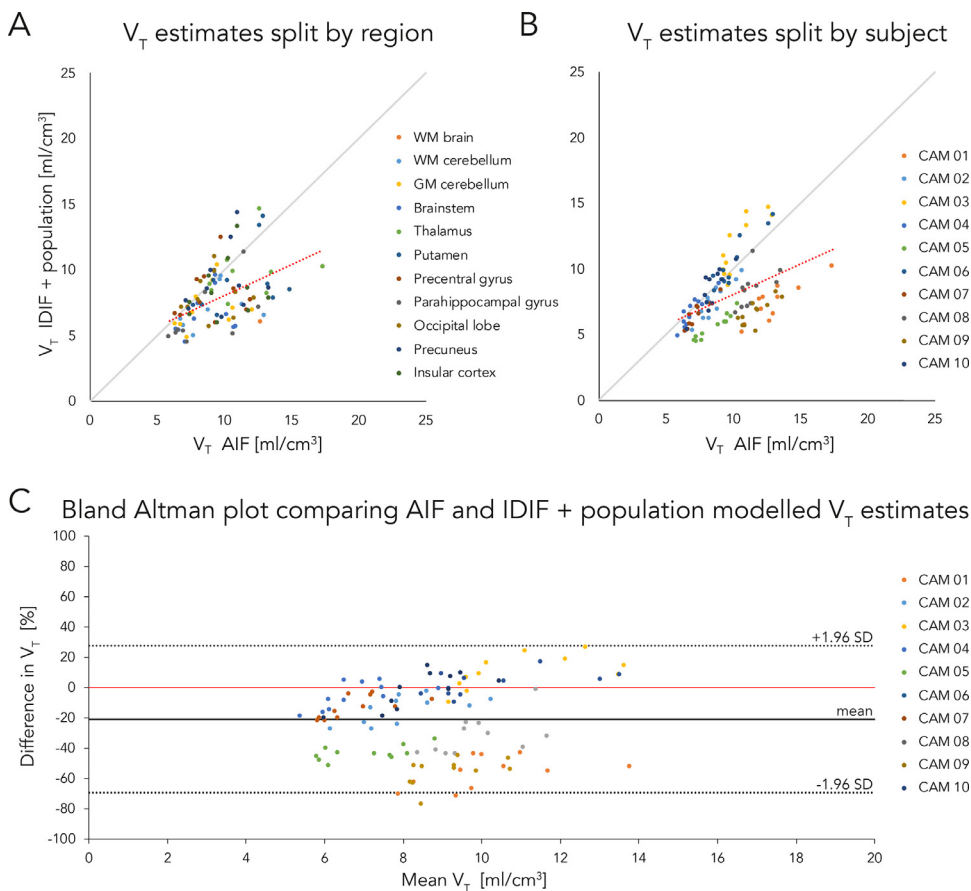
Fig. 7. Comparison of total volume of distribution estimates modelled with arterial or IDIF without venous samples input functions in healthy volunteers.

Scatter plots of total volume of distribution (V_T) estimates obtained with arterial (AIF) and IDIF without venous samples input functions are displayed in **panel A** (split by region) and **B** (split by subject). The red dotted line is the linear regression fit, the grey line indicates the line of unity. **Panel C** displays a Bland–Altman plot comparing V_T estimates modelled with arterial and IDIF without venous samples input functions. The thick black line is the mean bias of the V_T estimates modelled with an IDIF without venous samples input function, the dotted black lines denote the 95% confidence intervals. Please note that the range of the y-axis is different in this figure compared to Figs. 4C and 6C.

IDIF + population had higher coefficients of variation of V_T compared to arterial-based data (mean V_T CoV: arterial 21.3% ± 2.5% vs. IDIF + population 25.2% ± 4.1%, $t = 4.1$, $p = 0.002$).

3.5. Validation of venous-based correction factors in patients with traumatic brain injury

The demographic characteristics of the 7 TBI patients are given in Table 4. There was a high correlation between the AUC of the fits to arterial (mean 29 ± 12 min) and venous (mean 30 ± 12 min) parent fraction measurements ($r = 0.92$, $p = 0.003$, Fig. 8A). There was also a high correlation between the AUC of arterial (mean 113 ± 6 min) and venous (mean 111 ± 6 min) PWB ratio measurements ($r = 0.93$, $p = 0.003$, Fig. 8B), and between the 60-min arterial (1.98 ± 1.11 kBq/ml) and fitted venous (1.91 ± 1.13 kBq/ml) whole blood radioactivity concentrations ($r = 0.997$, $p<0.001$, Fig. 8C). The correlation with the measured 62-min venous whole blood radioactivity concentration was similarly high (1.91 ± 1.13 kBq/ml, $r = 0.997$, $p<0.001$).

Table 4
Characteristics of patients with traumatic brain injury.

ID	Injected activity [MBq]	Age [years]	Sex	Ethnicity	GCS	Mechanism	Interval between injury and scan	Medications at time of scan
TBI 01	186	62	M	European	3	Fall	4 days	Propofol, fentanyl
TBI 02	182	34	M	European	9	RTC	9 months	Metformin
TBI 03	178	37	M	European	6	RTC	9 months	Nil
TBI 04	170	32	M	European	8	Assault	3 days	Propofol, Fentanyl, Atracurium
TBI 05	200	18	M	European	6	RTC	7 days	Propofol, Fentanyl, Atracurium
TBI 06	204	44	M	European	5	RTC	7 days	Propofol, Fentanyl, Midazolam, Atracurium
TBI 07	192	54	F	European	4	Fall	16 months	Nil
Overview	Mean	Mean	86% Male	100%	Mean	57% RTC	Mean	57% Anaesthetics 43% No anaesthetics
	187 ± 12	40 ± 15	14% Female	European	6 ± 2	43% Other	151 ± 195 days	

GCS, Glasgow Coma Scale; M, male; F, female; RTC, road traffic collision.
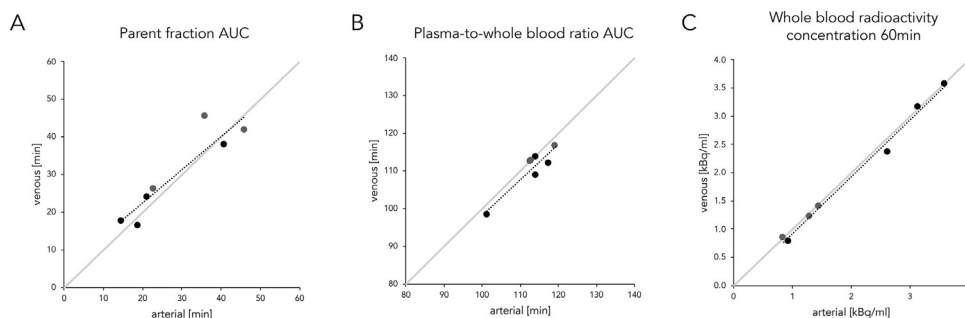
Fig. 8. Comparison of arterial and venous measurements in patients with traumatic brain injury.

Comparison of the area under the fitted curve (AUC) for arterial and venous parent fraction (**panel A**) and plasma-to-whole blood ratio (**panel B**), together with a plot of 60-min arterial vs. fitted venous whole blood radioactivity concentration (**panel C**) in patients with traumatic brain injury. Black dots denote patients that were receiving anaesthetic medications at the time of scan; grey dots denote patients that were not receiving anaesthetic medications at the time of the scan. The venous data used the five venous sample approach. On each plot the dotted line is the linear regression fit, the grey line indicates the line of unity.

4. Discussion

We present a novel method for quantification of [18F]GE-179 binding in brain that is independent of arterial sampling and might, thus, support wider use of this radiotracer for the assessment of the NMDA receptor. The tracer plasma input function estimated using a whole blood image-derived input function (IDIF) combined with corrections from five venous samples (i.e., parent fraction and PWB ratio) was highly correlated with the gold standard input function determined from arterial sampling. The mean bias in V_T estimates from the IDIF + 5 venous samples approach was small (< 2%) and the 95% limits of agreement were within a range (−15.9% to 12.4%) that would permit detection of differences seen with clinical diseases of at least 15–20%. Furthermore, the IDIF + 5 venous samples approach did not increase the variability of the V_T estimates. The performance of this procedure was superior to that provided by the IDIF combined with population-based corrections that did not utilise venous sampling, and that of previously proposed approaches aimed at obviating arterial sampling, namely the use of SUV or population-based input functions (McGinnity et al., 2018). However, simplification of the IDIF + venous method to use a single late venous measurement rather than data from five venous samples provided lower correlations and larger differences in V_T estimates.

Previous attempts to simplify [18F]GE-179 quantification using SUV or a population-based input function did not yield convincing results and both methods failed to reproduce differences in grey-matter V_T between patients with epilepsy and healthy volunteers (*p*>0.05) that were previously obtained using arterial modelled data on the same dataset (McGinnity et al., 2018). In addition, as there is no area of the brain devoid of NMDA receptors, there is no suitable reference region available for kinetic modelling. An alternative quantification approach is the estimation of an IDIF (Sari et al., 2017). However, an IDIF estimates radioactivity in whole blood and cannot determine the parent fraction of the tracer in plasma or the PWB ratio. We showed here that using the IDIF without any blood sampling did not provide accurate V_T estimates;

a methodology completely devoid of blood sampling will not provide an accurate input function for kinetic modelling unless the correction factors for parent fraction, PWB ratio and binding to plasma proteins are invariant across subjects. We chose to substitute arterial with venous samples and used venous data to determine the tracer parent fraction in plasma, the PWB ratio and to scale the IDIF. Binding to plasma proteins was found to be essentially invariant across subjects.

Previous studies found that venous samples taken with a longer delay after tracer injection provided better approximations of radioactivity in arterial blood (Takagi et al., 2004; Zanotti-Fregonara et al., 2012) and points to an increasing equilibrium between venous and arterial blood. In fact, the available evidence suggests there is little or no difference between venous and arterial radioactivity concentration more than 40–60 min after ligand injection (Meyer et al., 2005; Takagi et al., 2004; Wakita et al., 2000; Zanotti-Fregonara et al., 2012). Similarly, we found decreasing differences and increasing correlations between arterial and venous radioactivity concentration over time. The whole blood radioactivity concentration in a venous sample drawn 62 min after tracer injection was highly correlated with the 60-min arterial sample (*r* = 0.99 in healthy volunteers and *r* = 0.997 in patients with TBI). There remained a small underestimation of arterial data (mean difference −4% ± 2% in healthy volunteers and −5% ± 5% in patients with TBI) that was corrected using a linear model. Thus, we are confident that late venous whole blood radioactivity concentration provided a good estimate for calibrating the IDIF.

Greuter and colleagues performed an extensive evaluation of venous and arterial data (Greuter et al., 2011), correlating arterial and venous data obtained at 3 to 7 timepoints in studies with five different tracers with 254 paired samples overall. They observed differences in correlation coefficients between tracers and measured parameters (radioactivity concentration, parent fraction, PWB ratio) concluding that arterial samples cannot be readily substituted with venous measurements but require validation for each tracer and measured parameter.

We provide evidence that parent fraction, PWB ratio, and late whole blood radioactivity concentration can be reliably approximated using venous samples in [^{18}F]GE-179 PET. Similar correlations for late whole blood radioactivity concentration ($r \geq 0.99$) and PWB ratio ($r = 0.93$) were found for healthy volunteers and patients with TBI. The correlation for parent fraction was lower in patients with TBI ($r = 0.92$ vs. 0.99 in healthy volunteers), but still supported the feasibility of venous measurements.

The IDIF determined from the carotid arteries provided a similar shape to the input function determined from the radial artery. These data provide support that a previously proposed procedure correctly quantifies the radioactivity concentration in the carotid arteries (Sari et al., 2017). Residual differences between the arterial sampling and IDIF-based input functions can be explained by a higher noise and lower sampling rate in the imaging data for the first 6.5 min over which arterial samples were continuously sampled. The slight overestimation of radioactivity between 100 and 300 s after the injection for the IDIF could be due to spill-in effects from tracer uptake in brain or other tissue.

The combination of IDIF and data from 5 venous samples provided good estimates of the tracer plasma input function. This translated into high overall, regional, and subject-wise correlations of V_T estimates, with only minimal mean bias (−1.7%). These correlations were higher than those observed using SUV images or a population-based input function (McGinnity et al., 2018). The 95% limits of agreement of relative V_T differences ranged from −15.9% to 12.4%, which indicates that regional differences of more than 15–20% from control data could be defined as abnormal within individual patients. This is important and means that an IDIF and venous sampling approach for quantification of [^{18}F]GE-179 binding can be utilised to identify clinically relevant effect sizes within patient studies. In a population of patients with epilepsy not taking antidepressants scanned with [^{18}F]GE-179 PET we previously found a median whole brain V_T of 8.0 compared to a median V_T of 6.2 in healthy volunteers (McGinnity et al., 2015). This is a 29% difference in global V_T between patients and healthy volunteers, with significant focal V_T increases found within regions from four of 11 patients in the cohort. This suggests that such differences would be detected by our method and provides support for its practical applicability. Finally, there were no relevant outliers and there was no difference in overall data variability between the modelling techniques, providing further support for the robustness of the proposed method.

A reduction in the number of venous samples to only one late sample (62 min after tracer injection) provided less accurate estimates. This approach requires the use of population-based parameters in the functions fitted to the parent fraction and PWB ratio data, combined with a single parameter determined from the single venous sample. These estimates were less accurate than those obtained with a full set of venous samples, which translated into inaccuracies in input function and V_T estimates. There was significant bias in V_T estimates (mean difference 9.9%) and the 95% confidence intervals of V_T differences exceeded the 20% range, making this approach less reliable and not applicable for clinical use. Simplifying the method further to remove blood sampling altogether caused a significant degradation in accuracy, with V_T estimates correlating poorly with those from arterial sampling ($r = 0.45$). Hence, imaging without blood sampling cannot be recommended.

We confirmed the high correlation between arterial and venous parent fraction, PWB ratio, and late whole blood radioactivity concentration in a validation cohort of TBI patients. While the number of patients was small, it was a diverse group with four scans conducted within 7 days of severe injury on patients receiving anaesthetic medications to facilitate intensive care management at the time of scanning. The remaining three patients were scanned during follow up at 9–16 months post TBI. Thus, our method may be applicable to patients, and this includes those with physiological instability, and individuals who are receiving medications that could alter radiotracer metabolism.

In this work, we used two different PVC methods; one method (single target correction) for the IDIF estimation and another one (iterative Yang) for the brain radiotracer binding quantification. The reason for this is that iterative Yang requires segmentation of the whole image (which in the brain was provided by the GIF parcellation), while single target correction only requires a single region to be segmented (in this case the carotid arteries).

Another potential approach for estimating an input function from imaging data is simultaneous estimation (SIME), which estimates the input function by fitting multiple tissue activity curves from different brain regions (Sari et al., 2018). However, SIME involves the estimation of a large number of parameters that may lack precision, and could need scaling with one or more discrete blood samples (Feng et al., 1997). The application of SIME to [^{18}F]GE-179 PET will be the focus of future studies.

This study has limitations. We studied a small number of predominantly male adults scanned at a single centre due to the limited use of this radiotracer so far. While we were able to compare arterial and venous blood sampling in TBI patients we did not include other patient cohorts such as those with neuropsychiatric disorders. However, the large variability of tracer binding (V_T) in healthy subjects and the high correlation found between input function correction factors obtained from arterial and venous blood in both healthy volunteers and TBI patients makes us confident that the IDIF + venous approach may be generalisable to people with brain disorders taking medication. Our procedure requires venous sampling that is invasive and labour intensive. Puncture of the cubital vein is, nevertheless, less invasive and safer than placement of a cannula in the radial artery, and does not require such highly trained personnel. Estimation of the IDIF requires manual editing of the segmentation of the carotid arteries but this process could be automated in future (Jodas et al., 2016). The comparison of arterial and IDIF + venous data did not include correction for radioactivity bound to plasma proteins. However, data obtained from the arterial samples in both healthy volunteers and patients indicates that this correction, required to obtain the free tracer plasma input function, could be well approximated through a temporally-invariant 9% reduction of the tracer plasma input function. The IDIF component could not be assessed in TBI patients due to the lack of the necessary time-of-flight MRI. However, the accuracy of the IDIF is unlikely to differ significantly between healthy volunteers and patients, irrespective of the patient cohort. Using a group of 7 TBI patients, some of whom ($n = 4$) were studied during the acute phase of their illness and required anaesthesia to facilitate intensive care management, we demonstrated that changes in peripheral metabolism can be reliably captured using venous samples in patients as well as healthy volunteers.

To conclude, in healthy volunteers we validated a reliable method to quantify [^{18}F]GE-179 binding that does not require arterial sampling and showed that it may be applicable to patient cohorts such as those with TBI. A simplification of the method using a single venous sample rather than five provided less accurate estimates and should not be used, unless full venous sampling is either not available, or feasible. The single venous sample variant, however, provided superior results to one that did not utilise blood samples. In addition, we present evidence for reliable estimation of parent fraction, PWB ratio and late whole blood radioactivity concentration for this tracer using venous sampling. These approaches might widen the use of this tracer and the method could also be applied to other radiotracers, but this will require separate validation.

Credit authorship contribution statement

Marian Galovic: Conceptualization, Formal analysis, Data curation, Writing – original draft. **Kjell Erlandsson:** Conceptualization, Formal analysis, Data curation, Writing – original draft. **Tim D. Fryer:** Conceptualization, Funding acquisition, Formal analysis, Data curation, Writing – original draft. **Young T. Hong:** Conceptualization, Funding acquisition, Formal analysis, Data curation, Writing – original draft. **Roido Manavaki:** Funding acquisition, Writing – original draft. **Hasan Sari:**

Conceptualization, Formal analysis, Data curation, Writing – original draft. **Sarah Chetcuti:** Funding acquisition, Writing – original draft. **Benjamin A. Thomas:** Formal analysis, Data curation, Writing – original draft. **Martin Fisher:** Funding acquisition, Writing – original draft. **Selena Sephton:** Funding acquisition, Writing – original draft. **Roberto Canales:** Funding acquisition, Writing – original draft. **Joseph J Russell:** Funding acquisition, Writing – original draft. **Erik Årstad:** Conceptualization, Writing – original draft. **Franklin I. Aigbirhio:** Conceptualization, Writing – original draft. **Ashley M. Groves:** Conceptualization, Writing – original draft. **John S. Duncan:** Conceptualization, Writing – original draft. **Kris Thielemans:** Conceptualization, Formal analysis, Data curation, Writing – original draft. **Brian F. Hutton:** Conceptualization, Data curation, Writing – original draft. **Jonathan P. Coles:** Conceptualization, Funding acquisition, Formal analysis, Data curation, Writing – original draft. **Matthias J. Koepp:** Conceptualization, Formal analysis, Data curation, Writing – original draft.

Data availability

Funding

Disclosure/Declaration of Competing Interest

Acknowledgements

Supplementary materials

Supplementary material associated with this article can be found, in the online version, at doi:10.1016/j.neuroimage.2021.118194.

References

Bordji, K., Becerril-Ortega, J., Nicole, O., Buisson, A., 2010. Activation of extrasynaptic, but not synaptic, NMDA receptors modifies amyloid precursor protein expression pattern and increases amyloid-ß production. J. Neurosci. 30, 15927–15942. doi:10.1523/JNEUROSCI.3021-10.2010.

Cardoso, M.J., Modat, M., Wolz, R., Melbourne, A., Cash, D., Rueckert, D., Ourselin, S., 2015. Geodesic information flows: spatially-variant graphs and their application to segmentation and fusion. IEEE Trans. Med. Imaging 34, 1976–1988. doi:10.1109/TMI.2015.2418298.

Chen, K., Chen, X., Renaut, R., Alexander, G.E., Bandy, D., Guo, H., Reiman, E.M., 2007. Characterization of the image-derived carotid artery input function using independent component analysis for the quantitation of [18F] fluorodeoxyglucose positron emission tomography images. Phys. Med. Biol. 52, 7055–7071. doi:10.1088/0031-9155/52/23/019.

Cooke, S.F., Bliss, T.V.P., 2006. Plasticity in the human central nervous system. 129, 1659–1673. doi:10.1093/brain/awl082.

Erlandsson, K., Buvat, I., Pretorius, P.H., Thomas, B.A., Hutton, B.F., 2012. A review of partial volume correction techniques for emission tomography and their applications in neurology, cardiology and oncology. Phys. Med. Biol. 57, R119–R159. doi:10.1088/0031-9155/57/21/R119.

Erlandsson, K., Hutton, B., 2014. A novel voxel-based partial volume correction method for single regions of interest. J. Nucl. Med. 55, 2123 –2123.

Fan, M.M.Y., Raymond, L.A., 2007. N-methyl-D-aspartate (NMDA) receptor function and excitotoxicity in Huntington's disease. Prog. Neurobiol. 81, 272–293. doi:10.1016/j.pneurobio.2006.11.003.

Feng, D., Huang, S.C., Wang, X., 1993. Models for computer simulation studies of input functions for tracer kinetic modeling with positron emission tomography. Int. J. Biomed. Comput. 32, 95–110. doi:10.1016/0020-7101(93)90049-c.

Feng, D., Wong, K.P., Wu, C.M., Siu, W.C., 1997. A technique for extracting physiological parameters and the required input function simultaneously from PET image measurements: theory and simulation study. IEEE Trans. Inf. Technol. Biomed. 1, 243–254. doi:10.1109/4233.681168.

Greuter, H., Lubberink, M., Hendrikse, N.H., van der Veldt, A., Wong, Y., Schuit, R., Windhorst, A., Boellaard, R., Lammertsma, A., 2011. Venous versus arterial blood samples for plasma input pharmacokinetic analysis of different radiotracer PET studies. J. Nucl. Med. 52, 1974 –1974.

Gunn, R.N., Sargent, P.A., Bench, C.J., Rabiner, E.A., Osman, S., Pike, V.W., Hume, S.P., Grasby, P.M., Lammertsma, A.A., 1998. Tracer kinetic modeling of the 5-HT1A receptor ligand [carbonyl-11C]WAY-100635 for PET. NeuroImage 8, 426–440. doi:10.1006/nimg.1998.0379.

Hahn, A., Nics, L., Baldinger, P., Ungersböck, J., Dolliner, P., Frey, R., Birkfellner, W., Mitterhauser, M., Wadsak, W., Karanikas, G., Kasper, S., Lanzenberger, R., 2012. Combining image-derived and venous input functions enables quantification of serotonin-1A receptors with [carbonyl-11C]WAY-100635 independent of arterial sampling. NeuroImage 62, 199–206. doi:10.1016/j.neuroimage.2012.04.047.

Jodas, D.S., Pereira, A.S., R S Tavares, J.M., 2016. Lumen segmentation in magnetic resonance images of the carotid artery. Comput. Biol. Med. 79, 233–242. doi:10.1016/j.compbiomed.2016.10.021.

Kinahan, P.E., Rogers, J.G., 1988. Analytic 3D image reconstruction using all detected events. In: Proceedings of the Nuclear Science and Nuclear Power Systems Symposium.

Lipton, S.A., 2006. Paradigm shift in neuroprotection by NMDA receptor blockade: memantine and beyond. Nat. Rev. Drug Discov. 5, 160–170. doi:10.1038/nrd1958.

McGinnity, C.J., Hammers, A., Riaño Barros, D.A., Luthra, S.K., Jones, P.A., Trigg, W., Micallef, C., Symms, M.R., Brooks, D.J., Koepp, M.J., Duncan, J.S., 2014. Initial evaluation of 18F-GE-179, a putative PET Tracer for activated N-methyl D-aspartate receptors. J. Nucl. Med. 55, 423–430. doi:10.2967/jnumed.113.130641.

McGinnity, C.J., Koepp, M.J., Hammers, A., Riaño Barros, D.A., Pressler, R.M., Luthra, S., Jones, P.A., Trigg, W., Micallef, C., Symms, M.R., Brooks, D.J., Duncan, J.S., 2015. NMDA receptor binding in focal epilepsies. J. Neurol. Neurosurg. Psychiatr. 86, 1150–1157. doi:10.1136/jnnp-2014-309897.

McGinnity, C.J., Riaño Barros, D.A., Trigg, W., Brooks, D.J., Hinz, R., Duncan, J.S., Koepp, M.J., Hammers, A., 2018. Simplifying [18F]GE-179 PET: are both arterial blood sampling and 90-min acquisitions essential? EJNMMI Res. 8, 46. doi:10.1186/s13550-018-0396-2.

Meyer, P.T., Elmenhorst, D., Zilles, K., Bauer, A., 2005. Simplified quantification of cerebral A1 adenosine receptors using [18F]CPFPX and PET: analyses based on venous blood sampling. Synapse 55, 212–223. doi:10.1002/syn.20113.

R.K. Murrough, J.W., Iosifescu, D.V., Chang, L.C., Jurdi, Al, Green, C.E., Perez, A.M., Iqbal, S., Pillemer, S., Foulkes, A., Shah, A., Charney, D.S., Mathew, S.J., 2013. Antidepressant efficacy of ketamine in treatment-resistant major depression: a two-site randomized controlled trial. Am. J. Psychiatry 170, 1134–1142. doi:10.1176/appi.ajp.2013.13030392.

Olney, J.W., Newcomer, J.W., Farber, N.B., 1999. NMDA receptor hypofunction model of schizophrenia. J. Psychiatr. Res. 33, 523–533.

Pellock, J.M., Faught, E., Leppik, I.E., Shinnar, S., Zupanc, M.L., 2006. Felbamate: consensus of current clinical experience. Epilepsy Res. 71, 89–101. doi:10.1016/j.eplepsyres.2006.06.020.

Rothman, S.M., Olney, J.W., 1995. Excitotoxicity and the NMDA receptor–still lethal after eight years. Trends Neurosci. 18, 57–58. doi:10.1016/0166-2236(95)93869-y.

Sari, H., Erlandsson, K., Law, I., Larsson, H.B., Ourselin, S., Arridge, S., Atkinson, D., Hutton, B.F., 2017. Estimation of an image derived input function with MR-defined carotid arteries in FDG-PET human studies using a novel partial volume correction method. J. Cereb. Blood Flow Metab. 37, 1398–1409. doi:10.1177/0271678X16656197.

Sari, H., Erlandsson, K., Marner, L., Law, I., Larsson, H.B.W., Thielemans, K., Ourselin, S., Arridge, S., Atkinson, D., Hutton, B.F., 2018. Non-invasive kinetic modelling of PET tracers with radiometabolites using a constrained simultaneous estimation method: evaluation with 11C-SB201745. EJNMMI Res. 8, 58. doi:10.1186/s13550-018-0412-6.

Takagi, S., Takahashi, W., Shinohara, Y., Yasuda, S., Ide, M., Shohtsu, A., Seio, T., 2004. Quantitative PET cerebral glucose metabolism esti-mates using a single non-arterialized venous-blood sample. Ann. Nucl. Med. 18, 297–302. doi:10.1007/bf02984467.

Thomas, B.A., Cuplov, V., Bousse, A., Mendes, A., Thielemans, K., Hutton, B.F., Erlandsson, K., 2016. PETPVC: a toolbox for performing partial volume correction techniques in positron emission tomography. Phys. Med. Biol. 61, 7975–7993. doi:10.1088/0031-9155/61/22/7975.

Vibholm, A.K., Landau, A.M., Møller, A., Jacobsen, J., Vang, K., Munk, O.L., Orlowski, D., Sørensen, J.C., Brooks, D.J., 2020. NMDA receptor ion channel activation detected in vivo with [18F]GE-179 PET after electrical stimulation of rat hippocampus. J. Cereb. Blood Flow Metab. doi:10.1177/0271678X20954928.

Wakita, K., Imahori, Y., Ido, T., Fujii, R., Horii, H., Shimizu, M., Nakajima, S., Mineura, K., Nakamura, T., Kanatsuna, T., 2000. Simplification for measuring input function of FDG PET: investigation of 1-point blood sampling method. J. Nucl. Med. 41, 1484–1490.

Zanotti-Fregonara, P., Chen, K., Liow, J.-.S., Fujita, M., Innis, R.B., 2011a. Image-derived input function for brain PET studies: many challenges and few opportunities. J. Cereb. Blood Flow Metab. 31, 1986–1998. doi:10.1038/jcbfm.2011.107.

Zanotti-Fregonara, P., Liow, J.-.S., Fujita, M., Dusch, E., Zoghbi, S.S., Luong, E., Boellaard, R., Pike, V.W., Comtat, C., Innis, R.B., 2011b. Im-age-derived input function for human brain using high resolution PET imaging with [C](R)-rolipram and [C]PBR28. PLoS One 6, e17056. doi:10.1371/journal.pone.0017056.

Zanotti-Fregonara, P., Maroy, R., Peyronneau, M.-.A., Trébossen, R., Bottlaender, M., 2012. Minimally invasive input function for 2-18F-fluoro-A-85380 brain PET studies. Eur. J. Nucl. Med. Mol. Imaging 39, 651–659. doi:10.1007/s00259-011-2004-9.